Self-Diffusion and Tracer Diffusion in Sphere-Forming Block Copolymers

Kevin A. Cavicchi and Timothy P. Lodge*,†

Department of Chemical Engineering and Materials Science, University of Minnesota, Minneapolis, Minnesota 55455

Received May 22, 2003; Revised Manuscript Received July 29, 2003

ABSTRACT: The self-diffusion and tracer diffusion of asymmetric poly(ethylene-*alt*-propylene-*b*-dimethylsiloxane), PEP−PDMS, copolymers were measured using forced Rayleigh scattering. Diffusion measurements were made in the disordered state, in disordered micelles, and in the body-centered-cubic (bcc) sphere phase. The FRS intensity decays were fit with a single-exponential function in the disordered state and a stretched exponential function in disordered micelles and bcc spheres. The decays are interpreted as the diffusion of single chains with a broadened distribution of relaxation times when micelles are present, due to the polydispersity of chain lengths. The diffusion coefficients in disordered micelles and bcc spheres are retarded compared to the disordered state. This retardation is consistent with a hindered diffusion process, $D \sim D_0 \exp(-A\chi N_A)$, where χ is the Flory−Huggins interaction parameter, D_0 is the diffusion coefficient as χ approaches zero, and N_A is the length of the core block. The parameter A is found to increase as χN_A increases. These results are compared with recent experimental and computational work.

Introduction

Diblock copolymers can form different ordered nanostructures, depending on the relative length of the two blocks and the degree of segregation between them. The mobility of block copolymer chains within these phases can be significantly affected by these structures compared to the disordered state. Understanding the mechanisms of single chain diffusion will help build a framework for understanding various processes of interest, including the kinetics of structure formation and equilibration, and the frequency-dependent rheological properties.

Self-diffusion and tracer diffusion measurements have been reported in lamellar,[1−13] gyroid,[12,14] cylinder,[11,14,15] and body-centered-cubic (bcc) sphere phases.[11,16−18] To provide a consistent description of these various systems, it is helpful to resolve diffusion along an interface ("parallel") from diffusion across an interface ("perpendicular"), with diffusion coefficients D_{par} and D_{perp}, respectively. In macroscopically unoriented lamellae or cylinders, an isotropic D will represent some combination of D_{par} and D_{perp}. In oriented samples it has proven possible to determine D_{par} and D_{perp} separately.[4,8,10,11,14] However, when D_{perp} is significantly smaller than D_{par}, for example at moderate or high degrees of segregation, the presence of a small population of defects or misaligned domains can severely compromise accurate extraction of D_{perp}. On the other hand, in bcc spheres $D \approx D_{perp}$ because each chain must hop from sphere to sphere in order to diffuse. An advantage of measuring diffusion in bcc spheres is that it is possible to measure D_{perp} without having to macroscopically orient the domains or to deconvolute experimental signals to obtain D_{perp}, as in lamellar or cylinder samples.

In perpendicular diffusion the chain junction must depart from the interface for a chain to diffuse, thereby incurring an enthalpic penalty for pulling one block through the other domain. For this "hindered diffusion" mechanism the diffusion coefficient is given by[4,19]

$$D \sim D_0 \exp(-A\chi N_A) \tag{1}$$

where χ is the Flory−Huggins interaction parameter, D_0 is the diffusion coefficient in the absence of any interactions, i.e., as χ approaches zero, and A is a prefactor of order unity. The diffusion barrier is therefore proportional to the enthalpic penalty χN_A, where N_A is the number of monomers in the "foreign" block.

It has been suggested that the chains may adopt different transient conformations at large segregations to decrease the activation energy of diffusion. Two extremes have been proposed but have not yet been established experimentally. Helfand proposed that one block could stretch itself out to diffuse across the other domain.[20] In this hyperstretched state only part of the block would be exposed at one time to the other domain, thereby lowering the activation energy for diffusion. Rubinstein and Obhukov proposed that the foreign block could collapse into a globule.[21] In this case only the surface of a sphere is in contact with the other domain, shielding most of the foreign block from unfavorable contacts and also lowering the activation energy for diffusion.

Perpendicular diffusion has been measured before in block copolymers using a variety of techniques and in different morphologies. Dalvi and Lodge measured D_{perp} directly in macroscopically aligned lamellar poly(ethylene-*alt*-propylene-*b*-ethylethylene) by forced Rayleigh scattering.[4,10,11] Rittig et al. measured the diffusion coefficient in macroscopically unoriented poly(ethylene-*alt*-propylene-*b*-dimethylsiloxane) (PEP−PDMS) cylinders by pulsed field gradient NMR.[15] They were able to isolate D_{perp} by deconvoluting the experimental signal into parallel and perpendicular diffusion. Yokoyama and Kramer measured D_{perp} in poly(styrene-*b*-vinylpyridine) (PS−PVP) bcc spheres by forward recoil spectrometry.[17]

* Author for correspondence: e-mail lodge@chem.umn.edu.
† Also Department of Chemistry, University of Minnesota, Minneapolis, MN 55455.

10.1021/ma0346815 CCC: $25.00
Published on Web 08/26/2003

In each of these cases the diffusion could be described using the hindered diffusion mechanism, but the value of A varied among the different systems and with the magnitude of χN_A in the PS−PVP system.

Yokoyama et al. also simulated perpendicular diffusion in bcc spheres.[22] Using Langevin dynamics and a periodic potential field of amplitude α, they calculated D/D_0 as a function of α and N. The diffusion was found to follow the hindered diffusion mechanism, but where A increased with increasing αN_A.

Two additional studies of diffusion in bcc phases were made by Fleischer et al. in poly(styrene-*b*-isoprene) (PS−PI) spheres[16] and (PEP−PDMS) spheres[18] by PFG-NMR. In the PS−PI spheres two diffusive modes were observed, which were attributed to the diffusion of free diblock chains and chains fixed in micelles. The appearance of two modes is due to the short measurement time of the experiment (300 ms), in which the chains were unable to exchange completely between the free state and the micelle state. In the PEP−PDMS spheres below T_{ODT} there was one broad mode of diffusion. The distribution of diffusivities increases as the temperature was lowered. This mode was attributed to the diffusion of micelles rather than single chains.

This paper reports diffusion measurements for PEP−PDMS chains, both in the disordered state and in bcc spheres, over a range of χN_A ($2 < \chi N_A < 14$). The results are interpreted in terms of hindered diffusion (eq 1) and compared to the prior results and the recent simulations of Yokoyama et al.[22]

Experimental Section

Materials. Poly(ethylene-*alt*-propylene-*b*-dimethylsiloxane) diblock copolymers were polymerized by the sequential anionic polymerization of poly(isoprene-*b*-dimethylsiloxane) (PI−PDMS), followed by catalytic hydrogenation of the PI block. Isoprene (Aldrich) was stored over calcium hydride. It was further purified by stirring for 3 h each over dibutylmagnesium and *n*-butyllithium. Hexamethylcyclotrisiloxane (D_3, Aldrich) was stirred over calcium hydride for 4 h and dibutylmagnesium for 1 h at 90 °C. Cyclohexane was passed through silica and alumina columns. Tetrahydrofuran was passed through an alumina column. 1-*tert*-Butyldimethylsiloxypropyllithium (FMC Lithium Corp.) and chlorotrimethylsilane (Aldrich) were used as received. This initiator is used because it contains a hydroxyl group, protected by *tert*-butyldimethylsilyl (TBDMS) ether, which can later be used to attach a photochromic dye to create tracers for diffusion measurements. Isoprene was initiated with 1-*tert*-butyldimethylsiloxypropyllithium and reacted for 6 h at 40 °C in cylclohexane. A portion of the polyisoprene was cannulated out for molecular weight analysis. D_3 was added and stirred for 12 h at 25 °C to ensure complete initiation of the PDMS block. Sufficient tetrahydrofuran was added to make a 50:50 mixture of cyclohexane and tetrahydrofuran. PDMS was polymerized for 1.5 h (ca. 30% conversion) at 25 °C, when it was terminated with a 10-fold molar excess of chlorotrimethylsilane. The polymer was dried and redissolved in cyclohexane. The solution was washed with a 5% $NaHCO_3$ solution followed by repeated washings with deionized water. The polymer was precipitated in a 50:50 mixture of 2-propanol and methanol and dried under vacuum to constant weight. The polymer was then hydrogenated with $Pd/CaCO_3$ (Strem Chemical, unpoisoned, unreduced) using a standard procedure.[23]

A small amount of homopolymer PDMS was formed during the polymerization. This was removed by fractionation with toluene and methanol. The polymer-rich fraction was found to be free of any PDMS homopolymer by size exclusion chromatography (SEC) measurements in toluene. The molecular weight of the PI block was determined by SEC with THF as the mobile phase, using a light scattering detector (Wyatt DAWN), refractive index detector (Wyatt OPTILAB), and a dn/dc value for PI in THF of 0.124 mL/g.[24] The mole fractions of the blocks and the molecular weight of the PDMS block were determined using NMR. The resulting samples are denoted EPDMS($X-Y$), where X and Y refer to the PEP and PDMS block molecular weights in kilodaltons, respectively. The degree of polymerization for each polymer was determined on the basis of a common reference volume, equal to the geometric mean of the monomer molar volumes. The sample characteristics are listed in Table 1. The entanglement molecular weights, M_e, of PEP and PDMS are 1.5 and 12.0 kDa at 25 °C, respectively;[25] M_e increases slightly with increasing temperature for both monomers. Given that these polymers are predominately PEP, each of the polymers listed in Table 1 should be in the entangled state.

Table 1. Polymer Characteristics

polymer ID	M_n (kDa)[a]	f_{PEP}[b]	N	N_{PDMS}	PDI[c]	T_{ODT} (°C)[d]
EPDMS 11-1	12.1	0.90	177	17	1.04	<0
EPDMS 29-3	31.5	0.93	462	33	1.06	0
EPDMS 30-4	34	0.90	496	52	1.07	240
EPDMS 23-7	30	0.79	431	91	1.06	>300

[a] From SEC and NMR measurements. [b] From NMR measurements. [c] From SEC measurements. [d] From rheology measurements.

For a fraction of each polymer the TBDMS group of the initiator was deprotected to provide a hydroxyl functional group to attach a photochromic dye for diffusion measurements. The polymer was dissolved in tetrahydrofuran to form a 2 wt % solution. Hydrochloric acid (0.102 M) was added dropwise to make a 0.04 M solution. The solution was stirred for 2 days, after which methanol was added to precipitate the polymer. The polymer was dried, redissolved in cyclohexane, and washed with a 5% $NaHCO_3$ solution followed by repeated washings with deionized water. The success of the deprotection reaction was determined by NMR with deuterated chloroform as the solvent. There was a shift of the hydrogen peak on the carbon next to the oxygen at the chain end, from 3.55−3.60 ppm before deprotection to 3.60−3.65 ppm after deprotection.

The polymer was labeled by esterification of the hydroxyl group with 4′-(*N*,*N*-dimethylamino)-2-nitrostilbene-4-carboxylic acid) (ONS−COOH). The synthesis of ONS−COOH has been previously reported.[26,27] A typical reaction was as follows. 30 mL of methylene chloride was passed through an activated alumina column to remove any water. 200 mg of polymer, a 3-fold molar excess of ONS−COOH, and a 10-fold molar excess of both dicyclohexylcarbodiimide and (dimethylamino)pyridine were dissolved in the methylene chloride and refluxed at 50 °C for 2 days under nitrogen. The extent of the reaction was monitored using SEC with both a refractive index and a UV detector (Gilson model 166) at 360 nm. The labeled polymer was precipitated in methanol, redissolved in methylene chloride, and passed through a silica gel column to remove any unreacted dye. The labeled polymer was cloudy in appearance after drying. It was fractionated in toluene and methanol as described above, and the polymer-rich phase was recovered for use. From NMR measurements it was determined that the volume fraction of PDMS was not affected by the fractionation.

Forced Rayleigh Scattering. The diffusion coefficients were measured using forced Rayleigh scattering with an amplitude grating. The details of the experiment have been discussed previously.[4,28] FRS samples were prepared by mixing appropriate amounts of labeled and unlabeled polymer to make a sample with 5 wt % labeled polymer or 5 wt % tracer if the labeled polymer and the matrix were different. This mixture was dissolved in methylene chloride, filtered through a 0.45 μm filter, and precipitated in methanol. The polymer was dried to constant weight under vacuum and placed between circular glass slides separated by a 1 mm aluminum spacer. The sample was sealed with silicone sealant (GE) under an argon atmosphere. The fitting of experimental decays will be discussed subsequently.

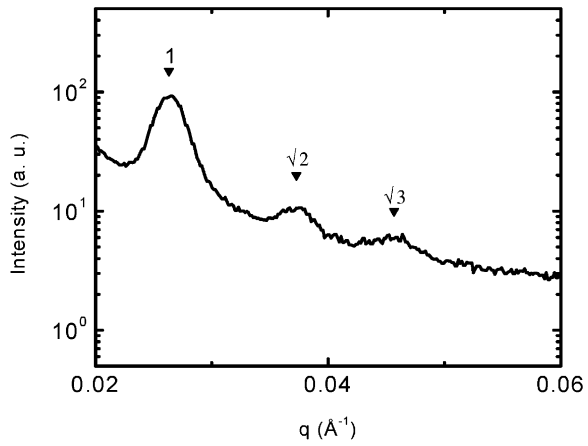

Figure 1. Azimuthally averaged SAXS intensity profile for EPDMS 30-4 at 100 °C. The peaks are at q/q^* values of 1, $\sqrt{2}$, and $\sqrt{3}$, indicating a bcc structure.

Small-Angle X-ray Scattering. Small-angle X-ray scattering experiments were performed using the 2 m SAXS line at the University of Minnesota. X-rays were generated using a rotating anode (Rigaku RU-200BVH) with a pinfocus cathode and collimated with a double-mirror configuration (Franks optics). 2-D patterns were recorded on a multiwire detector (Siemens). The sample-to-detector distance was kept at 230 cm. The sample temperature was controlled to within ±0.1 °C by resistive heaters mounted in a water-cooled brass block.

Rheology. Rheological measurements were carried out on an ARES rheometer (Rheometric Scientific) using 25 mm diameter parallel plates. The temperature was controlled to within ±1 °C using a nitrogen convection oven. Temperature ramps were carried out at $\omega = 0.5$ rad/s, a heating or cooling rate of 1 °C/min, and a strain amplitude of 0.5−2%.

Results and Discussion

This section is divided into three parts. The first addresses the phase behavior of the different samples used for diffusion measurements. The second describes the signals observed in the forced Rayleigh scattering experiments and their interpretation. The third part emphasizes the diffusion coefficients themselves. Self-diffusion measurements were made on EPDMS 11-1, EPDMS 29-3, and EPDMS 30-4. Measurements were also made using EPDMS 11-1 and EPDMS 23-7 as tracers diffusing in EPDMS 30-4.

Phase Behavior. SAXS was used to determine the morphology of each FRS sample. Figure 1 shows a typical azimuthally averaged intensity profile for EPDMS 30-4 at 100 °C. There are peaks at q/q^* ratios of 1, $\sqrt{2}$, and $\sqrt{3}$, which is consistent with the bcc sphere structure. SAXS profiles of the EPDMS 11-1 in EPDMS 30-4 and EPDMS 23-7 in EPDMS 30-4 samples are similar. Over the temperature range 20−180 °C, corresponding to the temperatures used in FRS, these three samples were all in the bcc sphere phase.

Both EPDMS 11-1 and EPDMS 29-3 showed no higher order peaks in SAXS measurements over the range 20−180 °C. Based on χ for EPDMS[29]

$$\chi = 64K/T - 0.03 \qquad (2)$$

$T_{ODT} = 240$ °C, and $N = 496$, the $(\chi N)_{ODT}$ for EPDMS 30-4 is 47. EPDMS 11-1 has the same f_{PEP} as EPDMS 30-4, and thus $(\chi N)_{ODT}$ should be similar. With a $(\chi N)_{ODT}$ of 47, T_{ODT} would be −60 °C for EPDMS 11-1. Given the lower values of χN over the temperature range of measurement, this polymer should therefore be disordered for all FRS measurements, consistent with the absence of higher order peaks in the SAXS results.

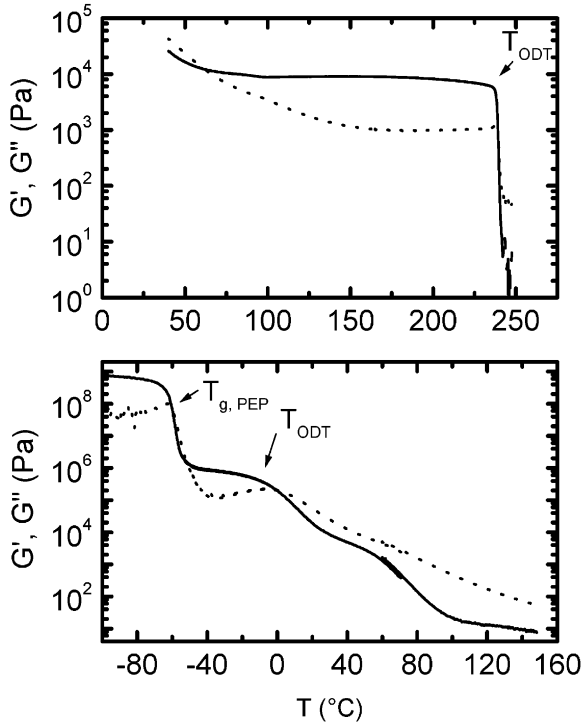

Figure 2. G', G'' vs temperature for (a) EPDMS 30-4 and (b) EPDMS 29-3: (—) G', (- - -) G''.

Rheology was also used to examine the phase behavior of the samples. Figure 2 shows temperature sweeps of G' and G'' for EPDMS 30-4 (Figure 2a) and EPDMS 29-3 (Figure 2b). The ODT for EPDMS 30-4 is marked by a precipitous drop in both G' and G'' at 240 °C. There is also a characteristic small peak in G'' before the ODT, as observed previously in bcc spheres, attributed to the softening of the lattice.[30,31] The ODT for EPDMS 29-3 is much broader, but there is still a peak in G'' and a drop in G', with T_{ODT} estimated to be 0 °C. The much more well-defined transition at −60 °C is the glass transition of the PEP block. There is a large temperature difference between the T_{ODT}'s for EPDMS 30-4 and EPDMS 29-3 even though the polymers have similar M_n's and f_{PEP}'s. However, these polymers have highly asymmetric volume fractions, where the phase boundary between bcc spheres and disorder is very steep with respect to the composition. EPDMS 29-3, with a higher volume fraction of PEP, has a larger $(\chi N)_{ODT}$. Above the ODT the frequency-dependent moduli for EPDMS 29-3 are not consistent with a fully disordered melt, and it is probable that the sample contains disordered micelles. Disordered micelles have been reported in disordered poly(styrene-*b*-isoprene) spheres above the ODT,[32−35] and in previous experiments on a different EPDMS copolymer with $f_{PEP} = 0.91$ disordered micelles persisted up to at least 280 °C, 105 °C above the T_{ODT}.[30] Given that the T_{ODT} of EPDMS 29-3 is approximately 0 °C, this system is expected to be in the disordered micelle state throughout the FRS measurements, especially at the lower temperatures.

In summary, these self-diffusion measurements correspond to the *disordered state* for EPDMS 11-1, to the *ordered state* for EPDMS 30-4, and to the *disordered micelle state* for EPDMS 29-3. The tracer diffusion measurements are all in the *ordered state*.

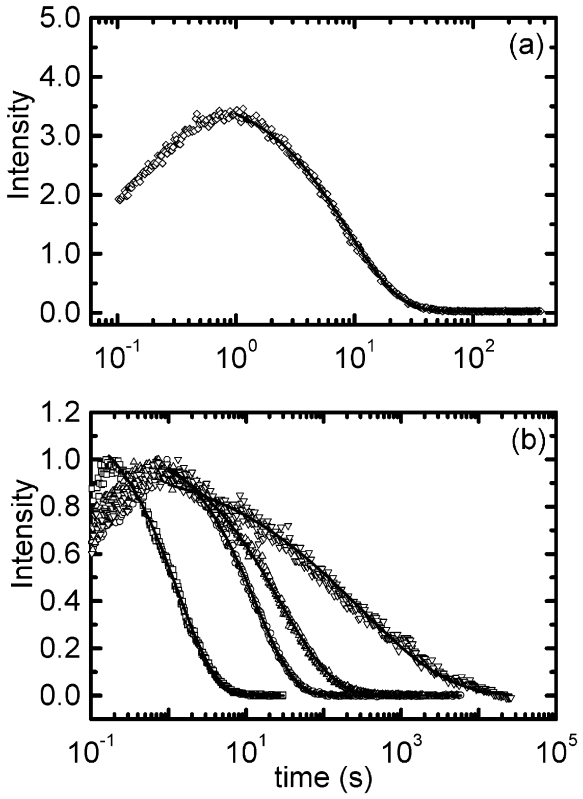

Figure 3. FRS intensity decays. (a) EPDMS 11-1 at 100 °C and $d = 10\ \mu$m. The solid line is a fit to the data using eq 3. (b) Decays at 100 °C: (□) EPDMS 11-1 in EPDMS 30-4, $d = 3.2\ \mu$m; (○) EPDMS 29-3, $d = 3.2\ \mu$m; (△) EPDMS 30-4, $d = 3.2\ \mu$m; (▽) EPDMS 23-7 in EPDMS 30-4, $d = 1\ \mu$m. The solid lines are fits to the data using eq 5.

FRS Signals. Figure 3 shows representative FRS decays for (a) disordered and (b) ordered polymers. In each trace the baseline has been subtracted, and the intensity has been normalized to a maximum value of 1 for clarity. Figure 3a shows a decay in EPDMS 11-1 at 100 °C and a grating spacing, d, of 10 μm. It could be fit with a single-exponential function

$$I(t) = (A \exp(-t/\tau))^2 + B \qquad (3)$$

where A is the amplitude, τ is the relaxation time, and B is the (incoherent) baseline. The fit was started after the peak in the intensity, which was typically at a time of 1 s or less. The origin of the initial intensity rise has been attributed to the photoisomerization of the dye.[36] It should be noted that the intensity rise was not always present in the decays, and there was no systematic dependence of its appearance on temperature, grating spacing, or sample. The full data set could also be fit to a double-exponential function

$$I(t) = (A \exp(-t/\tau_1) - C \exp(-t/\tau_2))^2 + B \qquad (4)$$

where τ_2 captures the initial intensity rise. The relaxation time τ_2 was not dependent on the grating spacing, indicating that this process was not diffusive in origin. Also, the diffusion coefficient determined from the single (τ) and double exponential (τ_1) fits did not differ by more than 10%.

Figure 3b shows signals for the four different ordered samples at 100 °C. They were all at a grating spacing of 3.2 μm, except for the EPDMS 23-7 in EPDMS 30-4 decay, which was at a grating spacing of 1 μm. A single exponential could not fit these decays, and instead a stretched exponential function was used

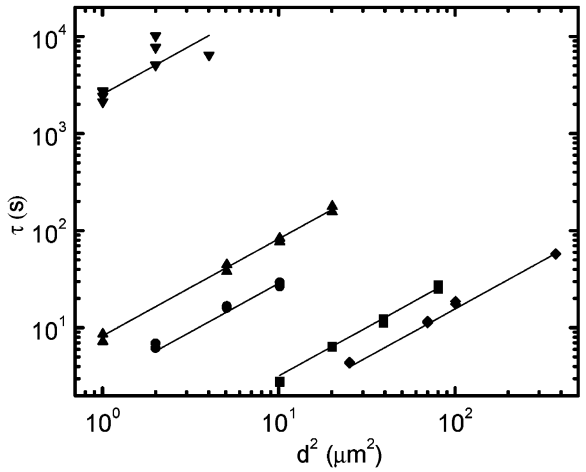

Figure 4. Relaxation time (τ) vs grating spacing squared (d^2) at 100 °C: (◆) EPDMS 11-1, (■) EPDMS 11-1 in EPDMS 30-4, (●) EPDMS 29-3, (▲) EPDMS 30-4, (▼) EPDMS 23-7 in EPDMS 30-4. The lines are fits to eq 6 for each data set.

$$I(t) = (A \exp(-(t/\langle\tau\rangle)^{\beta}))^2 + B \qquad (5)$$

where A is the amplitude, $\langle\tau\rangle$ is the mean relaxation time, β is related to the width of the distribution of relaxation times, and B is the incoherent baseline. The fits were also begun after the peak in the intensity. If a second exponential was used to fit the initial intensity increase, the resulting relaxation time for the rise was not dependent on the grating spacing. The diffusion coefficient from these fits was typically within 10% of the mean diffusion coefficient extracted from the stretched exponential ($\langle\tau\rangle$) fits.

Figure 4 shows the relaxation time, τ (or $\langle\tau\rangle$), vs the grating spacing squared, d^2, for each sample at 100 °C. The linearity of the data with a slope of 1 confirms the diffusive origin of the decays. This plot is also used to determine the diffusion coefficient, D, as

$$D = \frac{d^2}{4\pi^2\tau} \qquad (6)$$

The data were also plotted as $1/\tau$ vs $1/d^2$ and fit to determine D. The two values of D, which agreed well, were then averaged. Figure 5 shows the resulting diffusion coefficient measured for each sample as a function of temperature. The error bars indicate the 95% confidence interval determined from the τ vs d^2 fits. The error bar was omitted when the error was smaller than the symbol in the plot.

The stretched exponential fit can be interpreted as reflecting a single mode of diffusion with a broad distribution of relaxation times. We attribute the breadth of this distribution primarily to the polydispersity of the sample, convoluted via eq 1, as demonstrated below. In the disordered sample (EPDMS 11-1) the distribution caused by polydispersity is fairly narrow, and the data could be fit with a single exponential. In all the other samples there is a noticeable broadening of the distribution. If the mechanism is hindered diffusion, D will have a dependence on the core block length (via the exponent in eq 1) in addition to the dependence on total molecular weight (in D_0). Figure 6 shows the average β from the stretched exponential fit at each temperature vs χN_A.

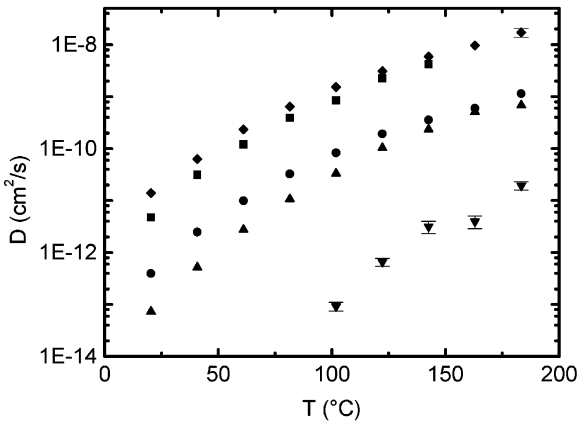

Figure 5. Diffusion coefficient (D) vs temperature: (◆) EPDMS 11-1, (■) EPDMS 11-1 in EPDMS 30-4, (●) EPDMS 29-3, (▲) EPDMS 30-4, (▼) EPDMS 23-7 in EPDMS 30-4.

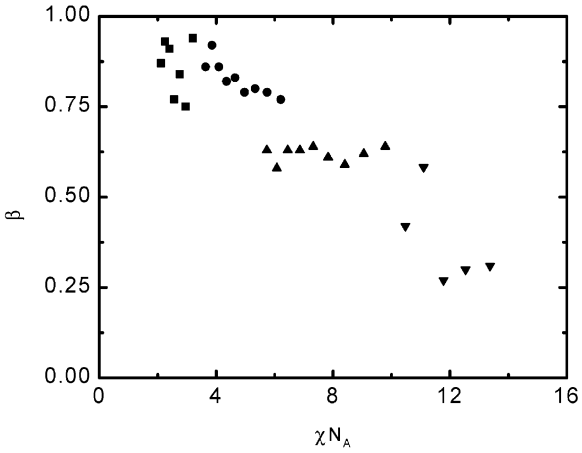

Figure 6. β vs χN_A: (■) EPDMS 11-1 in EPDMS 30-4, (●) EPDMS 29-3, (▲) EPDMS 30-4, (▼) EPDMS 23-7 in EPDMS 30-4.

Clearly, β decreases as the activation barrier increases, indicating a broader distribution with increasing activation energy.

To test this hypothesis further, the FRS decay of a polydisperse block copolymer was simulated. An average chain length, N_T, and volume fraction of the core block, f_A, were chosen. The distribution of block lengths was assumed to be Gaussian. The standard deviation of the distribution is related to the polydispersity (PDI) by

$$\sigma = N_T(\mathrm{PDI} - 1)^{1/2} \tag{7}$$

The concentration, c, of each chain length N is given by

$$c = K/[(2\pi)^{1/2}\sigma] \exp[-(N - N_T)^2/(2\sigma^2)] \tag{8}$$

where K is chosen such that, at $N = N_T$, $c = 1$.

Next, a temperature for the measurement was selected. $D_{0,N}$ for each chain length was calculated from the $D(T)$ of EPDMS 11-1, scaled to the appropriate molecular weight by the modified reptation result $D \sim M^{-2.3}$.[37] The mechanism of diffusion was assumed to be hindered diffusion, i.e., eq 1. The $\log(D/D_0)$ vs χN_A data shown in Figure 8 were fit to a third-order polynomial. Using this interpolation and $D_{0,N}$, D_N was calculated for each chain length.

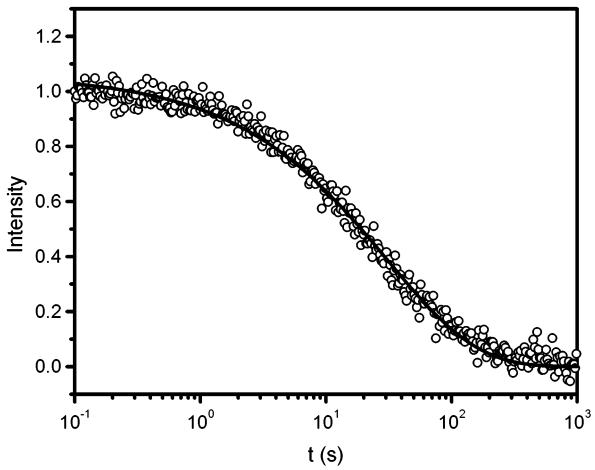

Figure 7. Simulated FRS intensity for EPDMS 30-4 at 100 °C and $d = 3.2$ μm. The solid line is a fit to a stretched exponential (eq 5).

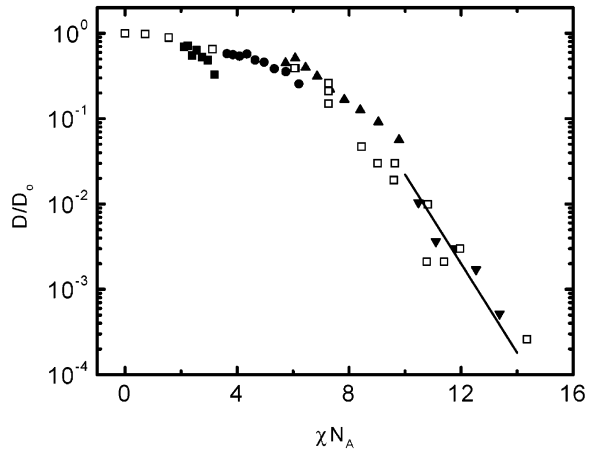

Figure 8. D/D_0 vs χN_A: (■) EPDMS 11-1 in EPDMS 30-4, (●) EPDMS 29-3, (▲) EPDMS 30-4, (▼) EPDMS 23-7 in EPDMS 30-4, (□) simulation of Yokoyama et al.[22] The straight line is a fit to the data of Yokoyama and Kramer.[17]

The simulated FRS intensity is given by

$$I = \sum_{N=50}^{2N_T}\left[c_N \exp\left(-\frac{4\pi^2 D_N t}{d^2}\right)\right]^2 \tag{9}$$

where t is the time and d^2 is the grating spacing. The summation was begin at $N = 50$ to avoid dealing with chain lengths below the entanglement chain length for PEP. The intensity contributions for these short chain lengths is very small, so their exclusion did not have an effect on the final intensity decay. The intensity was normalized, a baseline intensity was added, and noise was added to the data. The noise was randomly distributed about zero. Figure 7 shows the FRS intensity thus calculated for EPDMS 30-4 at $T = 100$ °C and $d = 3.2$ μm. A stretched exponential fit (eq 5) to the simulated data gives $\langle\tau\rangle = 97$ s and $\beta = 0.63$. The experimental decay shown in Figure 2b for EPDMS 30-4 is at the same temperature and grating spacing, where $\langle\tau\rangle = 82$ s and $\beta = 0.63$. Thus, we conclude that polydispersity can account for the broad distribution of diffusion coefficients, assuming that the diffusion is by hindered reptation. Also, the $\langle\tau\rangle$ from the fit is close to the relaxation time of the mean chain length and is therefore the appropriate moment to use in calculating the diffusion coefficient.

In a previous experiment on PS−PI copolymers two modes of diffusion were observed in bcc spheres.[16] The modes were attributed to the diffusion of free chains and of the spheres themselves. To resolve these two modes, the exchange time of chains between the free state and trapped state must be significantly longer than the measurement time. We therefore investigated whether a double-exponential fit could be used to fit our decays. In some cases a reasonable fit could be obtained, but in others it could not, and we therefore conclude that the stretched exponential is preferable.

Diffusion Coefficients. Figure 8 shows the normalized diffusion coefficient D/D_0 vs χN_A for each system. D_0 cannot be measured directly; instead, D_0 was estimated by from $D(T)$ of EPDMS 11-1 scaled to match the molecular weight of each tracer by

$$D_0 = D_{\text{EPDMS 11-1}}(M_{\text{tracer}}/M_{\text{EPDMS 11-1}})^{-2.3} \quad (10)$$

The temperature-dependent diffusivities of EPDMS 11-1 and a PEP homopolymer ($M_n = 16$ kDa) are identical after scaling $D_{\text{EPDMS 11-1}}$ by eq 10. Given that EPDMS 11-1 ($f_{PEP} = 0.90$) has a high PEP content, this implies that the diffusion of EPDMS 11-1 is not hindered, and therefore the reptation scaled EPDMS 11-1 data should give a good estimate of D_0. The data collapse rather well to a single master curve, spanning 4 orders of magnitude in reduced diffusivity. Also shown is a solid line, representing the PS−PVP data of Yokohama and Kramer as fit to the hindered diffusion model.[17] Excellent superposition is found between the two distinct systems (and two distinct experimental techniques) supporting the universality of eq 1. Note, however, that the curvature in the plot indicates that A in eq 1 varies with segregation strength. Finally, the open squares are the simulation results of Yokoyama et al.[22] In this case the simulation data were matched to the experimental data using the assumption that

$$\chi \approx 1.2\alpha \quad (11)$$

Yokoyama et al. remark that the conversion between α and χ is not trivial but that α is proportional to χ at strong segregations.

On the basis of these results, we conclude that the dominant mechanism of motion is hindered diffusion. First, the data agree well with the simulations of Yokoyama et al. Second, there is very good agreement with the data of Yokoyama and Kramer which were also interpreted as hindered diffusion. Third, there is no evidence of a transition to a different chain conformation to give a lower activation energy for diffusion. Such a transition would be observed as a weaker dependence of D/D_0 on χN. For the hyperstretched chain the diffusion coefficient should be[20]

$$D \sim D_0 \exp[-C(1 - f_A)(\chi N)^{2/3}] \quad (12)$$

where C is a constant. For asymmetric polymers this conformation should be extremely unfavorable because the activation energy is dependent on the size of the domain the chain is stretching across, which is large compared to the size of the core block.

For the collapsed sphere the diffusion coefficient is[21]

$$D = D_0 \exp[-E\chi^{1/2}(N_A)^{2/3}] \quad (13)$$

where E is a constant. Yokoyama and Kramer previously compared the barrier for hindered diffusion versus the collapsed sphere.[17] For the collapsed sphere they used the Helfand−Tagami form of the interfacial energy, valid at strong segregation.[38] The interfacial energy of the sphere, f, and therefore the activation barrier for diffusion is

$$\frac{f}{k_b T} = 4\pi\left(\frac{3}{4\pi}\frac{N_A}{\rho_0}\right)^{2/3} a\rho_0\sqrt{\frac{\chi}{6}} \quad (14)$$

where ρ_0 is the density and a is the segment length. As these authors noted, as this does not consider the entropy penalty for collapsing the chain, the activation energy from eq 14 is a lower bound. Using N_A of 100, the χ at the transition between mechanisms was approximately 0.3. For EPDMS 23-7, N_A is 95 and the maximum χ was 0.2, so a transition to a collapsed sphere would not be expected.

As a cautionary note, the good agreement between the PEP−PDMS and PS−PVP data in Figure 8 depends on the expression for χ. For symmetric PEP−PDMS various χ functions have been determined by one of two methods, as listed in Table 2. The first method was based on measurement of the T_{ODT} for two polymers and comparison with the predicted $(\chi N)_{ODT}$ from the theory of Fredrickson and Helfand.[39] The second method used small-angle neutron scattering (SANS) measurements of the disordered state structure factor.

It is not readily apparent why the χ determined from SANS is consistently larger than the χ value determined from T_{ODT}. Each different expression for χ would leave the D/D_0 vs χN_A plot qualitatively the same, but the superposition of our data with those of Yokoyama and Kramer could deteriorate somewhat.

In the simplest description of hindered diffusion, i.e., eq 1, the parameter A is a constant. That is clearly not the case experimentally, as the slope of D/D_0 vs χN_A increases as χN_A increases. Table 3 gives the apparent A value for each sample, assuming that eq 1 applies. One possible reason for the variation in A is the changing interfacial width of the sample. In weak segregation the composition profile is sinusoidal whereas in strong segregation it approaches a square wave. The interfacial width, w, should be dependent on χN, decreasing as χN increases. In the strong segregation regime w is predicted to be independent of N and proportional to $\chi^{-1/2}$.[38,42] At weaker segregations some of the core segments would already be in contact with corona block segments, and the enthalpic penalty to pull the core block out of the sphere should only be a fraction

Table 2. χ Values for PEP−PDMS

χ	MW polymer (kDa)	f_{PEP}	determination method
$64K/T - 0.03$	6.3, 7.7	0.48, 0.50	fit T_{ODT} (expt) vs χ_{ODT} (theory)[a]
$82K/T - 0.02$	6.6	0.50	SANS structure factor[b]
$98K/T - 0.06$	5.7	0.50	SANS structure factor[c]
$114K/T - 0.09$	7.8	0.50	SANS structure factor[c]

[a] Reference 29. [b] Reference 41. [c] Reference 40.

Table 3. Hindered Diffusion Fits to Diffusion Data

polymer sample	A
EPDMS 11-1 in EPDMS 30-4	0.56
EPDMS 29-3	0.27
EPDMS 30-4	0.50
EPDMS 23-7 in EPDMS 30-4	1.34

of χN_A. This adjustment to the hindered diffusion picture has been previously suggested, where D/D_0 would depend on χN_A as[43]

$$D/D_0 \sim \exp(-\Delta\phi A'\chi N_A) \quad (15)$$

where $\Delta\phi$ is the difference in volume fraction of B in the B-rich and A-rich domains. Thus, $A = \Delta\phi A'$ would increase as χN increases and thus as χN_A increases. This could also explain why A is larger than expected for the EPDMS 11-1 tracer. Since this is a tracer in EPDMS 30-4, w is determined by the more strongly segregated matrix.

However, the interfacial width can only provide a partial explanation for the variation in A. For example, for EPDMS 23-7 in EPDMS 30-4 an A of 0.5 would be expected, as in EPDMS 30-4 self-diffusion; this is not the case. Therefore, there is also an additional dependence of A on χN_A. This can also be seen directly in the simulation results in Figure 8, where the interfacial width was kept constant; as the potential is increased, A increases.

Conclusions

The diffusion coefficient of single chains has been measured in asymmetric PEP−PDMS copolymers over a wide range of χN_A. The diffusion was found to be retarded compared to diffusion in the disordered state and followed the hindered diffusion mechanism. The amount of retardation was found to increase as the activation barrier for diffusion increased. Good agreement was obtained between these results and recent experimental and simulation results, implying that this behavior is universal for asymmetric block copolymers.

Acknowledgment. This work was supported by the National Science Foundation, through Award DMR-9901087, and also by the Graduate School of the University of Minnesota, through a Doctoral Dissertation Fellowship (K.A.C).

References and Notes

(1) Shull, K. R.; Kramer, E. J.; Bates, F. S.; Rosedale, J. H. *Macromolecules* **1991**, *24*, 1383−1386.
(2) Ehlich, D.; Takenaka, M.; Okamoto, S.; Hashimoto, T. *Macromolecules* **1993**, *26*, 189−197.
(3) Ehlich, D.; Takenaka, M.; Hashimoto, T. *Macromolecules* **1993**, *26*, 492−498.
(4) Dalvi, M. C.; Lodge, T. P. *Macromolecules* **1993**, *26*, 859−861.
(5) Dalvi, M. C.; Eastman, C. E.; Lodge, T. P. *Phys. Rev. Lett.* **1993**, *71*, 2591−2594.
(6) Eastman, C. E.; Lodge, T. P. *Macromolecules* **1994**, *27*, 5591−5598.
(7) Hamersky, M. W.; Tirrell, M.; Lodge, T. P. *J. Polym. Sci., Part B: Polym. Phys.* **1996**, *34*, 2899−2909.
(8) Hamersky, M. W.; Tirrell, M.; Lodge, T. P. *Langmuir* **1998**, *14*, 6974−6979.
(9) Kannan, R. M.; Su, J.; Lodge, T. P. *J. Chem. Phys.* **1998**, *108*, 4634−4639.
(10) Lodge, T. P.; Dalvi, M. C. *Phys. Rev. Lett.* **1995**, *75*, 657−660.
(11) Lodge, T. P.; Hamersky, M. W.; Milhaupt, J. M.; Kannan, R. M.; Dalvi, M. C.; Eastman, C. E. *Macromol. Symp.* **1997**, *121*, 219−233.
(12) Rittig, F.; Kärger, J.; Papadakis, C. M.; Fleischer, G.; Almdal, K.; Štepánek, P. *Macromolecules* **2001**, *34*, 868−873.
(13) Fleischer, G.; Rittig, F.; Štepánek, P.; Almdal, K.; Papadakis, C. M. *Macromolecules* **1999**, *32*, 1956−1961.
(14) Hamersky, M. W.; Hillmyer, M. A.; Tirrell, M.; Bates, F. S.; Lodge, T. P.; von Meerwall, E. D. *Macromolecules* **1998**, *31*, 5363−5370.
(15) Rittig, F.; Fleischer, G.; Kärger, J.; Papadakis, C. M.; Almdal, K.; Štepánek, P. *Macromolecules* **1999**, *32*, 5872−5877.
(16) Fleischer, G.; Kärger, J.; Stühn, B. *Colloid Polym. Sci.* **1997**, *275*, 807−813.
(17) Yokoyama, H.; Kramer, E. J. *Macromolecules* **1998**, *31*, 7871−7876.
(18) Fleischer, G.; Rittig, F.; Karger, J.; Papadakis, C. M.; Mortensen, K.; Almdal, K.; Štepánek, P. *J. Chem. Phys.* **1999**, *111*, 2789−2796.
(19) Fredrickson, G. H.; Milner, S. T. *Mater. Res. Soc. Symp. Proc.* **1990**, *177*, 169−179.
(20) Helfand, E. *Macromolecules* **1992**, *25*, 492−493.
(21) Rubinstein, M.; Obukhov, S. P. *Macromolecules* **1993**, *26*, 1740−1750.
(22) Yokoyama, H.; Kramer, E. J.; Fredrickson, G. H. *Macromolecules* **2000**, *33*, 2249−2257.
(23) Bates, F. S.; Rosedale, J. H.; Bair, H. E.; Russell, T. P. *Macromolecules* **1989**, *22*, 2557−2564.
(24) Brandrup, J., Immergut, E. H., Grulke, E. A., Eds. *Polymer Handbook*, 4th ed.; John Wiley & Sons: New York, 1999.
(25) Fetters, L. J.; Lohse, D. J.; Richter, D.; Witten, T. A.; Zirkel, A. *Macromolecules* **1994**, *27*, 4639−4647.
(26) Ehlich, D. Diplomarbeit, Universität Mainz, 1984.
(27) Hamersky, M. W. Ph.D. Thesis, University of Minnesota, 1997.
(28) Chapman, B. R.; Lodge, T. P. *Trends Polym. Sci.* **1997**, *5*, 122−128.
(29) Vigild, M. E. Ph.D. Thesis, Riso Natl. Lab., 1997.
(30) Wang, X.; Dormidontova, E. E.; Lodge, T. P. *Macromolecules* **2002**, *35*, 9687−9697.
(31) Kim, J. K.; Lee, H. H.; Sakurai, S.; Aida, S.; Masamoto, J.; Nomura, S.; Kitagawa, Y.; Suda, Y. *Macromolecules* **1999**, *32*, 6707−6717.
(32) Sakamoto, N.; Hashimoto, T.; Han, C. D.; Kim, D.; Vaidya, N. Y. *Macromolecules* **1997**, *30*, 1621−1632.
(33) Han, C. D.; Vaidya, N. Y.; Kim, D.; Shin, G.; Yamaguchi, D.; Hashimoto, T. *Macromolecules* **2000**, *33*, 3767−3780.
(34) Schwab, M.; Stühn, B. *Phys. Rev. Lett.* **1996**, *76*, 924−927.
(35) Schwab, M.; Stühn, B. *Colloid Polym. Sci.* **1997**, *275*, 341−351.
(36) Milhaupt, J. Ph.D. Thesis, University of Minnesota, 2000.
(37) Lodge, T. P. *Phys. Rev. Lett.* **1999**, *83*, 3218−3221.
(38) Helfand, E.; Tagami, Y. *J. Polym. Sci., Part C: Polym. Lett.* **1971**, *9*, 741−746.
(39) Fredrickson, G. H.; Helfand, E. *J. Chem. Phys.* **1987**, *87*, 697−705.
(40) Schwahn, D.; Frielinghaus, H.; Mortensen, K.; Almdal, K. *Macromolecules* **2001**, *34*, 1694−1706.
(41) Schwahn, D.; Frielinghaus, H.; Mortensen, K.; Almdal, K. *Phys. Rev. Lett.* **1996**, *77*, 3153−3156.
(42) Helfand, E.; Tagami, Y. *J. Chem. Phys.* **1972**, *56*, 3592−3601.
(43) Lodge, T. P. In *Structure and Dynamics of Polymer and Colloidal Systems*; Borsali, R., Pecora, R., Eds.; Kluwer Academic Publishers: Dordrecht, The Netherlands, 2002; Vol. 568, pp 225−262.

MA0346815